



Deliverable



H2020 COMPET-05-2015 project ”Small Bodies: Near And Far (SBNAF)”

Topic: COMPET-05-2015 - Scientific exploitation of astrophysics, comets, and planetary data

Project Title: Small Bodies Near and Far (SBNAF)

Proposal No: 687378 - SBNAF - RIA

Duration: Apr 1, 2016 - Mar 31, 2019

WP	WP3: Lightcurve inversion technique
Del.No	D3.4
Title	Asteroid volume determination
Lead Beneficiary	AMU
Nature	Report
Dissemination Level	Public
Est. Del. Date	30 Sep 2017
Version	0.2
Date	02 Nov 2017
Lead Author	T. Santana-Ros; AMU (tonsan@amu.edu.pl)

WP3 Lightcurve inversion technique

Objectives: To join various types of data for full physical models of benchmark asteroids. To develop the web service with a database in order to provide the models to the community.

Description of deliverable D3.4

Shape and volume determinations for selected Gaia targets.

Scope of D3.4

The main goal of the deliverable is to provide a recipe for asteroid volume determination. In particular, we discuss the different shape models which can be used for volume estimate and the observation techniques which allow for their calibration. This knowledge will be applied to the so-called “Gaia perturbers” (GP). In this document we describe the state of the art of the photometric observation campaign carried out to model GPs and we compile the available thermal data and occultation timings which will be used to scale the shape models. We also provide some exemplary cases of the procedures developed to perform the volume determination.

Contents

1	Introduction	3
2	Observation techniques used for shape scaling	4
2.1	Radiometric techniques	4
2.2	Occultation timings	5
2.3	Other techniques: adaptive optics, radar echo, in-situ exploration	7
3	Shape models and calibration approach	8
3.1	Triaxial ellipsoid shape models	8
3.2	Convex shape models	10
3.3	Non-convex shape models	11
4	Observations of Gaia perturbers	12
4.1	Photometry	12
4.2	Stellar occultations	12
4.3	Radiometric techniques	13
5	Validation of the scaling techniques	14
5.1	Stellar occultations	14
5.2	Radiometric techniques	17
6	Discussion and conclusion	20
7	References	21
A	Appendix I	22

1 Introduction

In the last three decades a significant step forward has been taken to understand the nature of asteroids. With the use of modelling techniques, we have learned about their shapes and spin states. This knowledge has allowed us to better understand their formation and evolution. For instance, non-gravitational effects with a proven direct impact on asteroids' evolution such as YORP or Yarkovsky effects could not be understood without a precise knowledge of the shape and spin orientation of the asteroids studied.

The large majority of these models are based on relative photometric measurements. This technique is the main source of knowledge from asteroids as it provides their basic physical information such as rotation period and shape, or it can even allow for the discovery of satellites. Such observations, however, are not providing information about the size of the observed body. Relative photometry studies the relative variation in brightness of the asteroid in comparison to selected stars in the frame. As a result, the asteroid lightcurve obtained stands for the variation in brightness due to asteroid rotation, disregarding any other effects on the measured brightness, such as atmospheric or instrumental variations.

Other techniques are thus needed to scale the shape model, which allows for the determination of the asteroid's volume. One possible approach is to obtain direct measurements of the asteroid size such as the ones coming from timings recorded during stellar occultations or resolved images of the body gathered with large telescopes equipped with adaptive optics. It is also possible to estimate the size of these bodies by studying their radar echoes. These techniques, however, can only be applied to a limited set of asteroids (large Main Belt asteroids for the former and Near Earth Asteroids for the latter). On the other hand, thermal infrared data from space-based surveys is available for a great number of asteroids. On the basis of these data, it is possible to derive asteroid thermal models, which allow for their size estimate (i.e. radiometric diameters).

Asteroids in our Solar System can differ drastically in composition, as they can be a compound of metallic, rocky and/or icy material. Thus learning about their composition is essential to understand their physical nature, distribution, formation and evolution, leading to a better comprehension of how the Solar System formed and evolved. Besides a volume estimate, it is necessary to know the mass of the asteroid with good precision in order to calculate its bulk-density. It is, however, not straightforward to calculate the mass of an asteroid. Currently there are only few asteroids with a precise mass estimate (with <10% precision).

Fortunately, the Gaia mission (ESA) with its very accurate astrometric measurements, will provide some light in this topic. This space-based observatory will yield masses of more than one hundred asteroids (henceforth "Gaia perturbers") from gravitational perturbations during close approaches with other minor bodies. In particular, Mouret, Hestroffer & Mignard, (2007) found that at least 42 asteroid masses will be derived with a precision better than 10% and 150 with a precision better than 50%. With the aim of enhancing the exploitation of these data, we are conducting an observation campaign of a selected subgroup of these asteroids. With the new data gathered, we will be able

to derive their detailed shape models and spin states. It will be then possible to scale these models using stellar occultations or thermal models, which in turn will allow for an unprecedentedly precise bulk-density estimate.

In this document we describe the techniques and observations that we plan to use for a volume estimate of the “Gaia perturbers” (GP). At first, we plan to derive shape (convex, non-convex) and spin-state solutions (unique or mirror pole solutions, but reliable rotation periods) of a subset of the GP list. Next we will scale these shape solutions combining them with occultation techniques or radiometric techniques. For the scaled shape models obtained, it will be possible to derive reliable values of their density. This requires the availability of high-quality masses, which will be provided by the Gaia mission (data expected for the final mission release, scheduled for end 2022). In Sec. 2 we describe the known observation techniques for asteroid size estimate, paying particular attention to the techniques of our expertise (thermal modeling and stellar occultations). Next, Sec. 3 discusses the three-dimensional shape models which can be used for volume estimate. The state of the art of the photometric observation campaign of GPs and a compilation of their available thermal data and occultation timings is provided in Sec. 4, while exemplary cases of volume estimate are given in Sec. 5.

2 Observation techniques used for shape scaling

2.1 Radiometric techniques

The radiometric technique uses (simple or more complex) shape/spin models to derive the size, albedo, and thermal properties from measurements of the object’s thermal emission. A detailed description of the capabilities and limitations of this technique can be found in Delbo et al. 2015 and references therein. The quality of the derived properties depends on:

- the quality and quantity of the available thermal (infrared/submm/mm) measurements (coverage in wavelengths, phase angles before/after opposition, rotational phases, etc). See Deliverable 6.6, Sec. 2.
- the reliability of the shape and spin-state solution for the object
- the validity of the thermal/thermophysical model which is used to interpret the data

The disk-integrated thermal emission of an asteroid at a given observing and illumination geometry is a very reliable proxy for the size of the object (see very slowly increasing line for the thermal constraint in Fig. 1): (i) the thermal measurements (of e.g. large main-belt asteroids) are usually very accurate, often better than 10% in absolute flux accuracy; (ii) the thermal emission originates from the entire hemisphere (illuminated warm parts and non-illuminated colder regions); (iii) the thermal emission is connected to the thermal properties of the surface regolith (usually low-conductivity fine-grain dust layer like on the lunar surface), while surface mineralogy and colours play only a secondary role. The radiometric size determination (see Fig. 1) was already applied to many thousand asteroids (based on IRAS, MSX, ISO, Spitzer, AKARI, Herschel, WISE/NEOWISE, etc. IR surveys and dedicated observations) and validated against sizes derived from other techniques (occultation & AO imaging) and in-situ measurements (see also earlier deliverables of WP6).

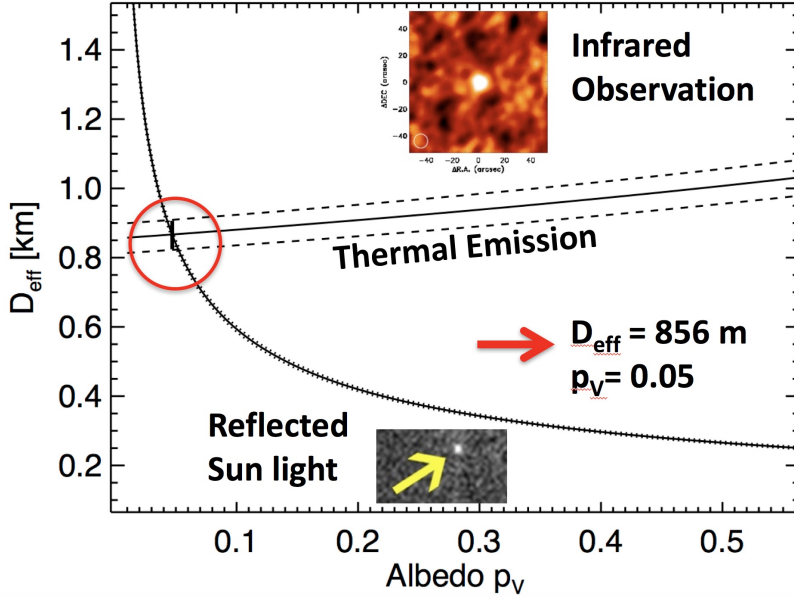


Figure 1: The figure illustrates the radiometric technique: the combination of reflected light and thermal emission allows to solve for size and albedo simultaneously. The example shows is based on the work by Müller et al. 2017 on the Hayabusa-2 mission target 162173 Ryugu. Measurement of the thermal emission (solid and dashed straight lines) put very strong constraints on the object’s size.

As a rule of thumb one can translate a 10% accuracy of a measured absolute infrared flux into a 5% error for the derived radiometric size, at least for cases where reliable shape and spin solutions are available, and where the thermal measurements allow to constrain well the objects’ thermal properties.

A crucial point for the radiometric technique is the accuracy of the object’s rotational state at the time of the thermal measurement. Using shape solutions which are ”out of phase” can lead to poor radiometric sizes (note, that there are usually no thermal lightcurves available to do the phasing directly against the measurements). Therefore, we use in our analysis always a given convex/non-convex solution (with the corresponding spin-state and the specified zero points in rotational phase and time) and a spherical shape solution with the same spin-state solution. This allows us to see if the true shape solution is indeed leading to a better fit of all thermal measurements simultaneously (lower values in χ^2 , see discussions in Marciniak et al. 2017). This exercise also helps to get confidence in size solutions where no (or only poor) shape/spin solutions are available.

2.2 Occultation timings

One of the main ground-based techniques to obtain information of the asteroid’s size consists in recording the time of a stellar occultation due to the asteroid’s transit from the observer’s point of view. In addition, if several observers at different positions within the shadow path measure accurately the timing and duration of the dimming at their locations, a 2D snapshot of the shape of the object can be reconstructed by projecting these recorded times

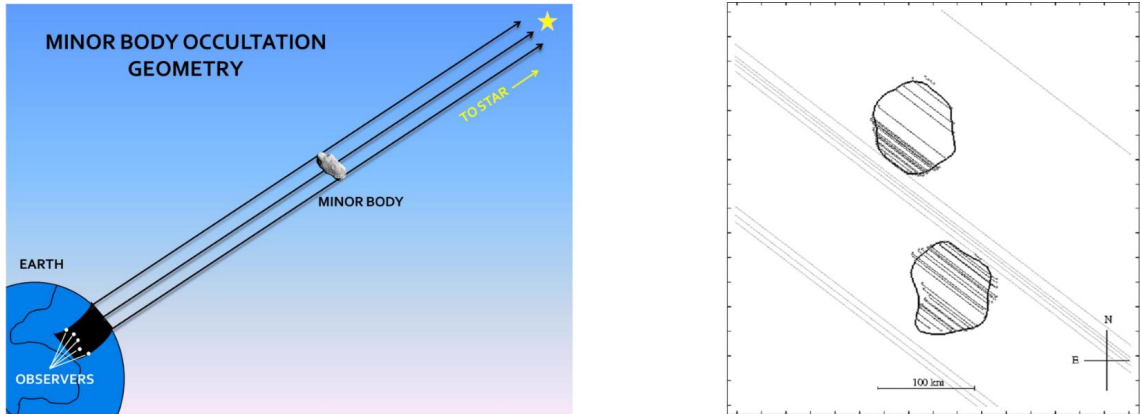


Figure 2: *Left panel: schematic of a stellar occultation (adapted from Santos-Sanz et al. 2016). Right panel: the impressive set of chords obtained by Colas et al. (2012) for the binary asteroid (90) Antiope and its companion. The silhouettes are the best-fitting, non-convex shape model derived by Bartczak et al. (2014) from lightcurve (LC) inversion using the SAGE algorithm.*

on the plane of the sky, which produces segments called chords. This technique, that may seem unsophisticated, results in an invaluable opportunity to obtain direct observations of the body size and shape, and unlike other observing techniques, it can help retrieving information of small-class asteroids (as long as the accuracy of their orbit is good enough to predict the event). This is because we are not directly observing the asteroid, but the brightness of the occulted star. An occultation may still be observed and timed even if the asteroid itself is too faint to be seen!

A nice description of the stellar occultation technique and its exploitation for asteroid modeling was provided in Deliverable 6.1: Occultation vs thermal tools. In short, an occultation of a star by an object such as an asteroid takes place when the object crosses the observer’s line of sight to the star. As a consequence, the brightness of the star diminishes during the event. Any extended object will produce a shadow whose projection on the Earth retains its size because the stars are effectively at infinity. If we aim to scale an asteroid’s shape model – e.g. coming from relative photometry – we can therefore project the asteroid’s snapshot onto the occultation chords at the epoch of the event (a schematic view is shown in Fig. 2). In order to look for the best fit of the model’s silhouette to the chords, we have developed a procedure that moves the model in x and y axes (i.e. on Earth’s surface) and scales it looking for the minimum possible residual between model and observations (see examples provided in Bartczak et al. 2014, 2017, and Marciniak et al. 2017). As a result, we obtain a scaled shape model, for which we can compute its volume.

Interestingly, the publication of the complete Gaia catalogue will improve greatly the accuracy of occultation predictions; in particular, it will reduce the uncertainty in the track of the shadow path thus allowing more accurate planning and coordination of observations. The expected improvement in prediction accuracy will result from the much greater precision in star positions and proper motions that Gaia will produce, as well as (in the final release scheduled for end 2022) much better determination of the asteroids’ orbits. The early data releases from Gaia are already being incorporated into the prediction software used by

occultation observers. Eventually it is hoped that shadow paths may be predicted with an accuracy of 1 km. A mid-size telescope (i.e. 1 meter telescope) will potentially observe from a single site between 20 and 40 events for such objects per year.

In addition to the size and shape applications, occultations may also provide serendipitous discoveries, e.g. in the form of binary asteroids (when a secondary component is observed in the occultation timings) or ring systems, as the ones discovered around the Centaur Chariklo (Braga-Ribas et al. 2014) or around the trans-Neptunian dwarf planet Haumea (Ortiz et al. 2017).

2.3 Other techniques: adaptive optics, radar echo, in-situ exploration

The observing techniques described above are the main source of model scaling in our project. There are, however, other methods which also allow for asteroid size estimate. We briefly describe them below.

- Adaptive optics (AO) correct in real-time for the atmospheric turbulence and provide diffraction-limited near-infrared images. AO images of large asteroids can be used similarly to occultation chords in order to scale the shape model. It is possible by ground-based AO instrumentation to resolve several main-belt asteroids which are very close to the diffraction limit of an 8-10 m telescope (typically ~ 60 mas, corresponding to main-belt asteroids with $D > 50$ km). Knowing the angular size and the distance to the asteroid, we can use these observations to scale its shape model following a similar recipe than the one described for stellar occultations. More advanced methods allows also for extracting information not only from the silhouette, but also from the inner part of the resolved image, so to include information of the large concavities in the modeling process. This is the case of ADAM inversion method (Viikinkoski, Kaasalainen & Durech 2015a), which iteratively improves the solution by minimizing the residuals between the Fourier transformed images and a projected polyhedral model. The resulting shape model is therefore scaled, allowing for its volume calculation. For further details on AO observations of asteroids see Deliverable 6.5: "Ground truth" shape models, and references therein.
- Asteroid radar image is a reconstruction of a radio signal sent from the Earth and reflected by body's surface. For this reason, this technique is best working for objects approaching the Earth, such as NEOs. One dimension of such image comes from time delay, as the signal has to travel different distances depending on which part of asteroid's surface it is reflected from. Second dimension is directly associated with body's rotation. Received echo's frequency is shifted with respect to incident ray due to Doppler effect and depends on radial velocity of a surface element which increases as we move away from asteroid's rotation axis. Range of frequency shift depends on asteroid's rotation period and aspect (angle between rotation axis and direction to the observer). As a result one can produce range-Doppler image where each pixel value corresponds to echo power at certain distance and radial velocity. Knowing the physics behind radar observations, allows us to generate synthetic radar observations with the asteroid's shape model (Fig. 3). By confronting model with observations it is possible to constrain the size of the asteroid and to calculate its volume.

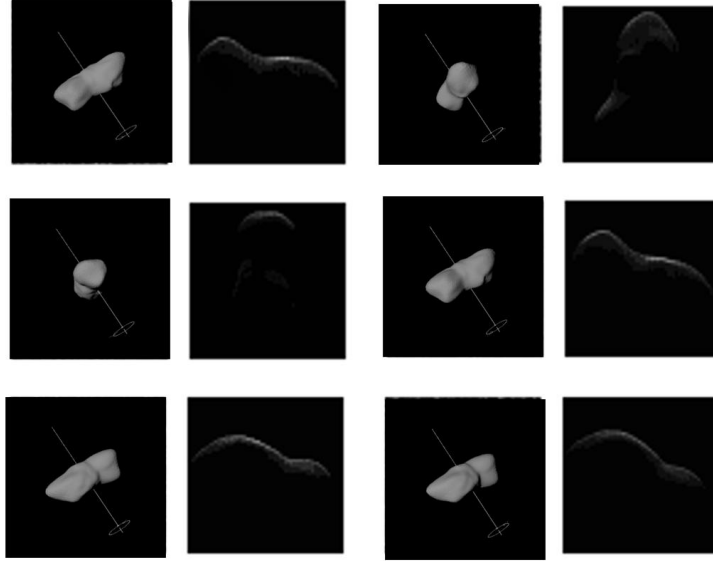


Figure 3: *Comparison of range-Doppler images of 1996 HW1. First and third column: simulated asteroid model as seen by observer; second and last column: simulated range-Doppler image (figure adapted from Santana-Ros, Dudziński & Bartczak 2017).*

- Space mission fly-bys and rendezvous are a rare opportunity to study a targeted asteroid *in situ*. The advantages of obtaining such observations are obvious – highly detailed information of the asteroid, potentially available for any asteroid size and location, etc – but the enormous cost of such missions reduces the list of visited asteroids to one dozen. Yet the information gathered during these missions are very useful for testing ground-based methods. In particular, knowing with high accuracy the size of the visited asteroids, allows us to validate the methods used for asteroid’s size determination described above. A nice description of the asteroids visited by space missions and the resulting science was provided in Deliverable 6.3: In-situ object properties.

3 Shape models and calibration approach

3.1 Triaxial ellipsoid shape models

A 3-axis ellipsoid shape can be a fairly good approximation for the majority of cases to describe the magnitude variation of an asteroid due to its change in geometry from the observer point of view (Connelly and Ostro 1984, Michałowski 1993, Torppa et al. 2008). Such ellipsoid can be defined as the region bound by a surface given by the equation:

$$(x/a)^2 + (y/b)^2 + (z/c)^2 = 1 \quad (1)$$

where a, b and c are the semi-axes and satisfy the condition $a \geq b \geq c$. An example of an ellipsoid in the principal axis spin state (c axis coincident with the spin axis) is shown in Fig. 4.

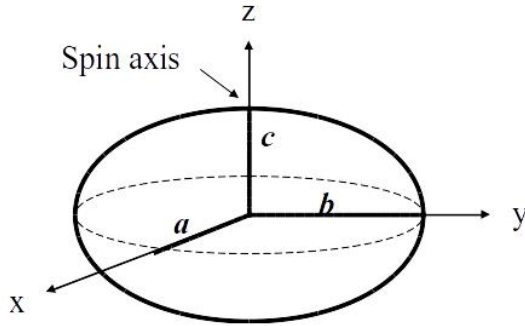


Figure 4: *An ellipsoid defined in a given reference frame rotating about its spin axis in principal axis spin states.*

Most of the asteroids show two maxima and two minima per rotational cycle. Such a lightcurve can be explained considering an ellipsoidal shape rotating about its spin axis (λ , β) in principal axis spin state with a given sidereal period (P), as shown in Fig. 5. The shape of the ellipsoid is then defined by two parameters, namely, the ratios of the lengths of the principal axes ($\frac{b}{a}$ and $\frac{c}{a}$). A model relying on such a representation of shape is completed with an initial rotation angle ϕ_0 and the sense of rotation of the body (prograde or retrograde). Using these parameters, it is possible to explain the variation in brightness of an asteroid, not only due to a rotation itself, but also due to the changes of the viewing geometry for the Sun–*Gaia*–asteroid system. Analytically, the brightness of the asteroid at a given time t , is proportional to the surface area seen from a given reference frame (cross-section of the asteroid presented to the observer). The cross-section can be calculated using the following equation:

$$S = \pi \sqrt{\frac{e^t Q e}{\det Q}} \quad (2)$$

where e is the unit vector pointing from the asteroid to *Gaia*, and $\det Q = \frac{1}{a^2 b^2 c^2}$.

As we change the rotation angle ϕ , so does the cross-section observed, thus we obtain a sinusoidal variation on the brightness, as seen in Fig. 5.

A spherical body representation can be considered as a particular case of the ellipsoidal shape, where $\frac{b}{a} = \frac{c}{a} = 1$. Such shape model cannot reproduce photometric lightcurves with a non-zero amplitude (considering homogeneous albedo), and thus cannot be used to derive the spin-state of the asteroid. However, if the spin-state is known, this simple shape model can be very useful in thermal modeling, as it gives a good estimate of the radiometric size and it can be used to evaluate the goodness of complex (e.g. convex and nonconvex) shape models of the asteroid.

Pros: Can give a fair solution of the inversion problem for poor datasets, e.g. sparse photometric measurements from astrometric surveys. As the inversion solution is purely analytic, it is easy to compute large datasets, such as the *Gaia* photometric catalogue of

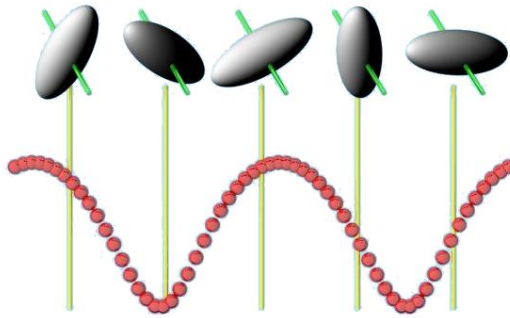


Figure 5: *A sinusoidal lightcurve can be explained based on the rotation of an ellipsoid.*

asteroids to be published at the end of the mission. The spherical solution is often used in thermal modeling with good results.

Cons: The main constraint of the triaxial shape models is that they fail to reproduce non-sinusoidal lightcurves produced by asteroids with very irregular shape. Besides, they can be useful for studying spin states, but the solution provides very limited information about the real shape of the asteroid (only some vague idea of the body elongation).

3.2 Convex shape models

Some lightcurve shapes cannot be explained by the use of a simple triaxial ellipsoid model. Asteroids with complex shapes can produce lightcurves with three or more maxima per cycle. In the majority of cases these asteroids are modelled using a convex representation of their real shapes (Kaasalainen & Torppa 2001, Kaasalainen, Torppa & Muinonen 2001), which despite being a first-order approximation of the real shape of the body (e.g. Fig. 6), have been proven to be good enough to fit the lightcurves and to derive asteroid's main physical parameters. In short, this method attempts to fit a set of parameters namely:

- A convex shape represented as a collection of triangular facets
- Sidereal rotation period
- Pole direction
- Albedo-dependent coefficient for Lommel-Seeliger and Lambert scattering laws

The standard solution of the inversion problem consists in minimizing the residuals between disk-integrated photometric data and synthetic brightness generated by the model. The process relies on the Minkovski minimization stability of convex bodies (Lamberg 1993) which makes the method not very sensitive to random noise in data. This inversion technique has been used by several authors during the last decade (e.g. Āurech et al. 2007, Marciniak et al. 2011, 2012) resulting in around two hundred of convex asteroid models based on dense lightcurves.

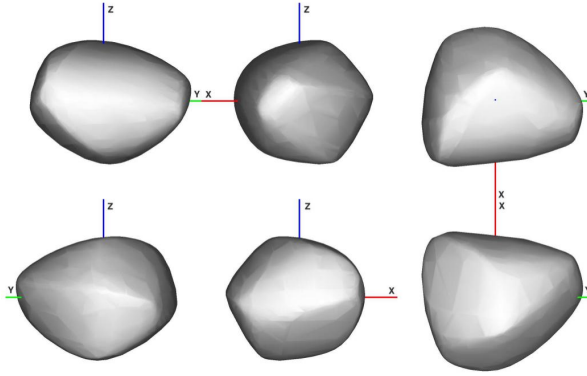


Figure 6: *A convex shape model of 478 Tergeste from Marciniak et al. 2017.*

Pros: This shape representation can successfully reproduce the majority of lightcurves observed. The inversion process is purely analytic, which means that is low CPU demanding (when the period is known).

Cons: Mathematical shape solution. The resulting shape model can have a spin axis direction which differs several degrees from the principal axis of inertia. This means that the shape model is not physical, and thus can differ from the real shape of the body. In case of asteroids with very irregular shapes, their convex representation can present poor fit to direct measurements, such as stellar chords.

3.3 Non-convex shape models

From direct images of asteroids obtained by radar, adaptive optics or during space missions like NEAR Shoemaker or Hayabusa, we know that the real shapes of asteroids are not convex, but generally are full of concavities. In order to obtain a more accurate shape model, alternative methods have been proposed. For instance, Bartczak & Dudziński 2017 recently developed a new inversion method called SAGE (Shaping Asteroids with Genetic Evolution) capable to derive nonconvex shape models for single and binary asteroids relying on their disk-integrated photometric measurements. In this case, the optimization problem is tackled by a genetic algorithm, which randomly mutates the model parameters and selects the best trial solutions until the evolution stabilizes. These models confirm the pole directions and rotation periods derived with previous methods, and additionally can provide a more realistic representation of the real shape of the asteroid (e.g. Fig. 7).

Pros: Physical shape solution. Can be used to study asteroids with irregular shapes, providing a better fit to direct measurements.

Cons: Their calculation is CPU demanding. There is no sense to use such models for low quality photometry or sparse data.

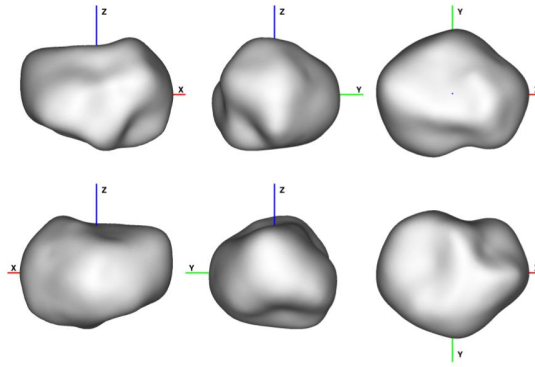


Figure 7: A nonconvex shape model of 9 Metis from Bartczak & Dudziński (2017).

4 Observations of Gaia perturbers

4.1 Photometry

The volume estimate of an asteroid is an intermediate step to its bulk density estimate. To calculate the latter, it is necessary to know the mass of the body. At present, there are only few asteroids for which a precise mass has been derived. One of the techniques used for mass determination is based on astrometric measurements taken before and after close encounters between a massive asteroid and a smaller one. The astrometric precision provided by Gaia allows for the measurement of tiny gravitational perturbations of a hundred of asteroids, which will lead to their mass determination with a precision better than 10% (Mouret, Hestroffer & Mignard, 2008). These precise measurements will result in an unprecedented improvement of the dynamical modelling of the Solar System and will have a direct impact on our knowledge of the physics of asteroids.

These targets are therefore perfect candidates for volume estimate. Combining both knowledges (mass from Gaia and volume from shape models) we can derive their bulk density. For this reason, we have selected a sub-sample of the Gaia perturbers (criteria are defined in Deliverable 6.4: Gaia asteroid list) and we have undertaken a photometric observation campaign to obtain their shape models. The campaign status is summarized in Table 1. This table gathers information on the quality of the existing shape model, the number of apparitions observed, the dates of SBNAF observations and whether these data are enough or not to derive a nonconvex shape model.

4.2 Stellar occultations

For the list of selected GPs, we have compiled from the Planetary Data System (Dunham et al. 2017) the timings from available stellar occultations. These data will be used to scale the shape models derived using the photometric data gathered in our observation campaign. A first estimate of the asteroid size, however, can be already done projecting a simple ellipsoid to the chords. In Appendix I, we summarize the available stellar occultations for the selected GPs, including their observation date, number of chords and the size and the angle of the semi-axes of the ellipsoid fitting the timing segments. For the majority of our

Asteroid	Current shape model code	Apparitions observed by SBNAF (year)	Total number of apparitions observed	Enough data for high quality model
13 Egeria	C	2016	8	Yes
14 Irene	D	2015 – 2016 – 2017	13	Yes
20 Massalia	D	2016	11	Yes
60 Echo	D	–	5	No
64 Angelina	D	2016 – 2017	12	Yes
68 Leto	D	2016	6	No
113 Amalthea	E	–	4	No
114 Cassandra	–	2016	8	No
145 Adeona	–	2016	7	Yes
162 Laurentia	D	2016 – 2017	7	No
297 Caecilia	D	2017	9	Yes
308 Polyxo	–	2016	5	No
381 Myrrha	D	2016 – 2017	7	Yes
402 Chloe	D	2016	7	Yes
441 Bathilde	D	2017	9	No
636 Erika	D	2017	4	No
654 Zelinda	–	2017	7	Yes
704 Interamnia	E	2016 – 2017	12	Yes
721 Tabora	–	2016	3	No
1427 Ruvuma	–	2017	5	No
1626 Sadeya	–	2016	5	No

A – Asteroids with detailed up to a small-scale shape model (high resolution models from in situ imaging)
B – Asteroids with a medium-scale shape details (a non-convex model which converges with the convex solution)
C – A first-order shape model, like a unique convex solution, based on dense lightcurves
D – A low-resolution first-order (“angular”) shape model based on mainly sparse data or on limited dense data
E – A triaxial ellipsoid unique shape model

Table 1: *State of the art of the GP observation campaign.*

targets we have found stellar occultations with positive chords (18 out of 20). However, only 13 asteroids have multi-chord occultations (more than 2 positive chords), allowing for a size determination. The majority of observed occultations have only one or two chords, which can be only used to constrain the minimum size of the observed asteroid. This is not enough for our purposes considering the final goal of this exercise – to derive accurate densities of GPs. On the other hand, it worth noting the impressive coverage for the occultations of 381 Myrrha (25 positive chords) and 704 Interamnia (46 positive chords).

4.3 Radiometric techniques

In Deliverable 6.4 we described the available thermal data from space telescopes¹ for the full GPs list. WISE and AKARI data are available for all the asteroids in the selected

¹IRAS, MSX, ISO, Planck, Herschel, WISE and AKARI

subset. For the majority of targets, we can also rely on data from IRAS (18 out of 20). Unfortunately, the high quality thermal data coming from Herschel is only available for two of them (20 Massalia and 704 Interamnia).

5 Validation of the scaling techniques

In this section we aim to provide practical examples of the procedures we plan to follow in order to derive the volume of GPs. In particular, we focus on the techniques we are more experienced with, i.e. stellar occultations and radiometric techniques. For the former, we study the case of three asteroids (9 Metis, 159 Aemilia and 329 Svea), while for the latter we have used seven exemplary cases (6 Hebe, 9 Metis, 159 Aemilia, 227 Philosophia, 329 Svea, 478 Tergeste and 487 Venetia). Convex and nonconvex shape models are taken from three publications (Marsset et al. 2017, Marciniak et al. 2017 and Bartczak & Dudziński 2017). However, we have added the case of the simple spherical shape model with the goal of studying the influence of the shape model used on the volume estimate.

5.1 Stellar occultations

For each of the three asteroids studied, we have fitted three different shape models (sphere, convex and nonconvex) to the available multi-chord occultations. As a result, the models have been scaled in kilometers, allowing for the calculation of its volume. The uncertainty of the fit is calculated with the root mean square deviation (RMSD) between model and observations, following

$$RMSD = \sqrt{\frac{1}{n} \sum_i^n (\hat{y}_i - y_i)^2}, \quad (3)$$

where n is the number of chords, y_i is the longitude of a positive chord and \hat{y}_i is the longitude of a segment crossing the model in the direction of the chord.

For simplicity when comparing the models, we express the size of the asteroids in terms of the diameter of the equivalent volume sphere.

- 9 Metis

For this asteroid we found two multi-chord occultations (from 2008 and 2014) with very rich coverage of the body’s 2D shape. The equivalent volume sphere diameters (EVSD) resulted to be very similar for all the shape models. In both occultations, however, the nonconvex shape model provided the best fit in terms of rmsd. Importantly, the residual of the sphere shape model resulted to be about twice as large as the one obtained for the nonconvex solution. Due to error propagation, the uncertainty found when calculating the sphere volume is even larger – almost three times the uncertainty of the nonconvex shape. Fits of the different models to the chords are shown in Fig. 8 and Fig. 9, while Table. 2 summarizes the results obtained.

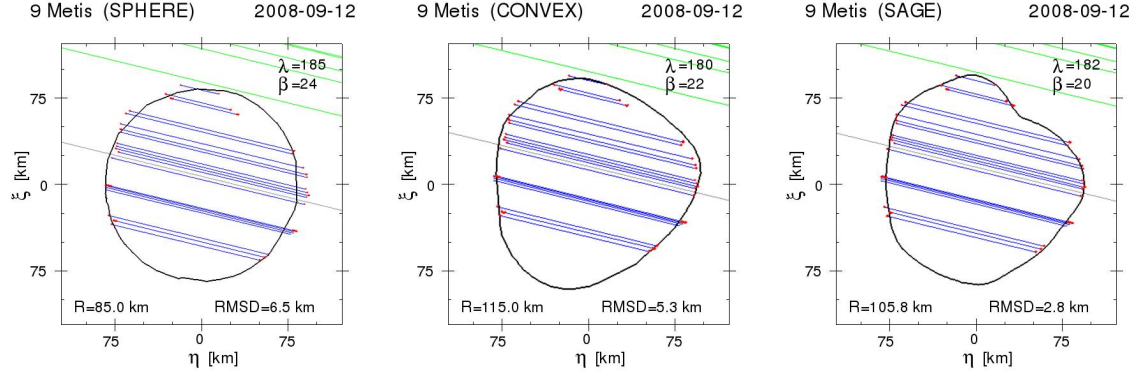


Figure 8: Three different shape solutions of 9 Metis fitted to 2008 occultation. The R is the size of the model, i.e. the length of the longest vector in the model, based on the fit.

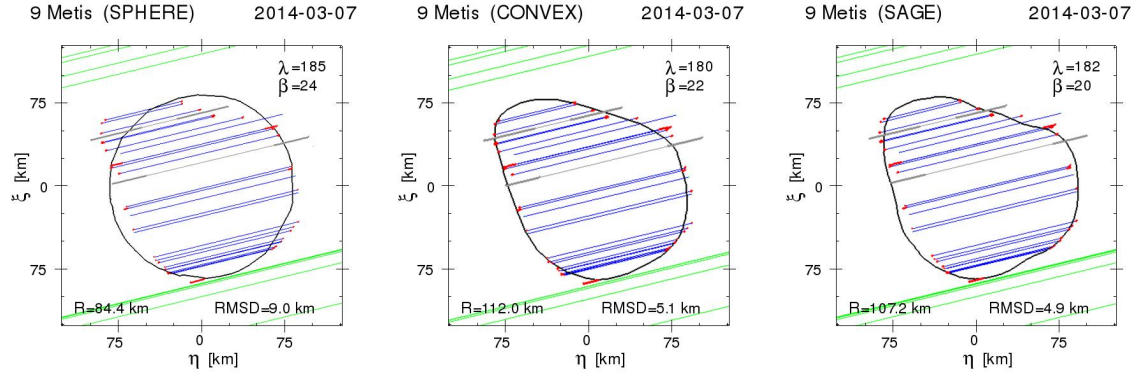


Figure 9: Three different shape solutions of 9 Metis fitted to 2014 occultation. The R is the size of the model, i.e. the length of the longest vector in the model, based on the fit.

Shape model	EVSD [km]	Volume [m^3]
9 Metis – 2008		
Sphere	170 ± 13	$(2.57 \pm 0.59) \cdot 10^{15}$
Convex	170 ± 7	$(2.56 \pm 0.33) \cdot 10^{15}$
Nonconvex	165 ± 5	$(2.56 \pm 0.20) \cdot 10^{15}$
9 Metis – 2014		
Sphere	169 ± 18	$(2.52 \pm 0.81) \cdot 10^{15}$
Convex	165 ± 8	$(2.36 \pm 0.31) \cdot 10^{15}$
Nonconvex	167 ± 8	$(2.43 \pm 0.34) \cdot 10^{15}$

Table 2: Diameter and volume determination of 9 Metis for three different shape models and two independent occultations.

- 159 Aemilia

In this case, convex and nonconvex solutions gave similar results, but the sphere shape model clearly overestimated the diameter (and consequently, the volume) of the asteroid. Fig. 10 shows the fit of the different shape models, while Table 3 summarizes the results obtained.

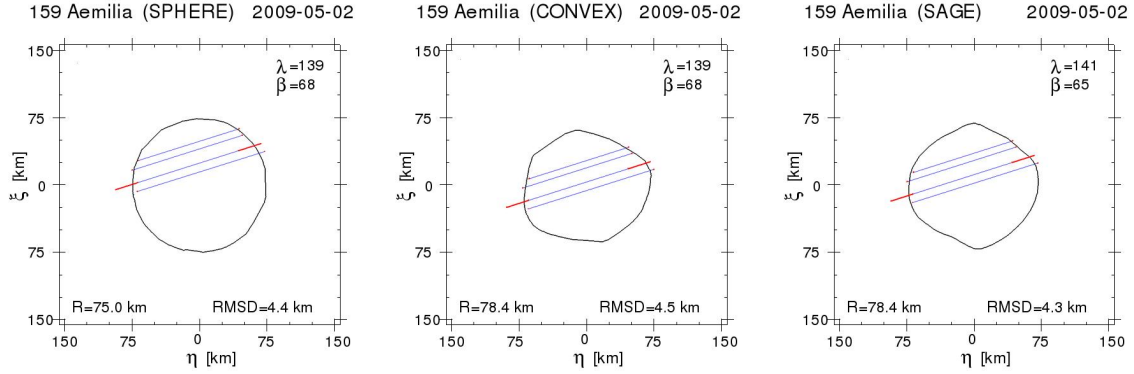


Figure 10: *Three different shape solutions of 159 Aemilia fitted to 2009 occultation. The R is the size of the model, i.e. the length of the longest vector in the model, based on the fit.*

Shape model	EVSD [km]	Volume [m^3]
159 Aemilia – 2009		
Sphere	150 ± 9	$(1.77 \pm 0.62) \cdot 10^{15}$
Convex	130 ± 7	$(1.14 \pm 0.31) \cdot 10^{15}$
Nonconvex	135 ± 7	$(1.28 \pm 0.34) \cdot 10^{15}$

Table 3: *Diameter and volume determination of 159 Aemilia for three different shape models and two independent occultations.*

- 329 Svea

A similar situation was founded with this asteroid. Although all the diameters obtained are comparable within their error, the uncertainty on the volume derived with the sphere shape model was about twice the nonconvex uncertainty. Fig. 11 shows the fit of the different shape models, while Table 4 summarizes the results obtained.

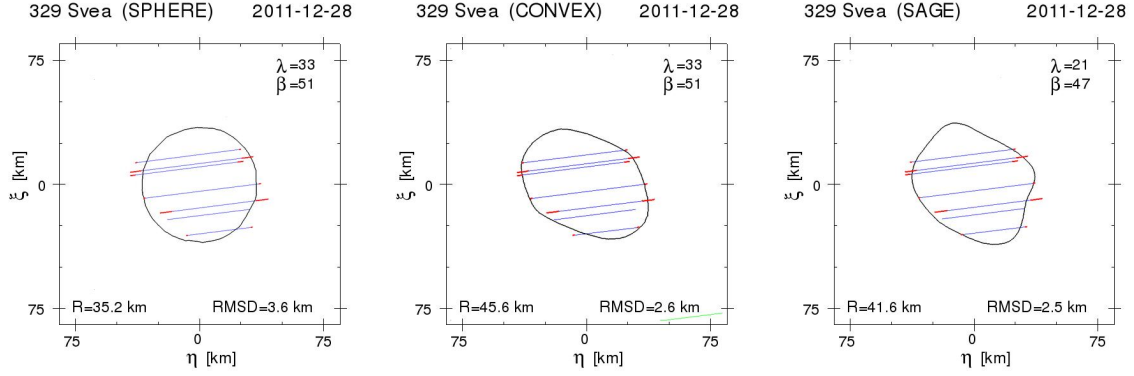


Figure 11: Three different shape solutions of 329 Svea fitted to 2011 occultation. The R is the size of the model, i.e. the length of the longest vector in the model, based on the fit.

Shape model	EVSD [km]	Volume [m^3]
329 Svea – 2011		
Sphere	70 ± 7	$(1.83 \pm 0.56) \cdot 10^{14}$
Convex	72 ± 4	$(1.95 \pm 0.33) \cdot 10^{14}$
Nonconvex	70 ± 4	$(1.80 \pm 0.31) \cdot 10^{14}$

Table 4: Diameter and volume determination of 329 Svea for three different shape models and two independent occultations.

5.2 Radiometric techniques

Radiometric sizes are typically accurate on a 5% level (for the given multi-epoch, multi-phase, multi-wavelength thermal data set). Often, the radiometric analysis favours a specific spin-axis orientation (see also Deliverable 6.6: Thermally resolved shape models), although sometimes both solutions produce similar-quality fits to the thermal data depending on the thermal data coverage of the object’s northern and southern hemisphere. In some cases there are very wide ranges of thermal inertias compatible with the available thermal data, usually when the before/after opposition situation is not well balanced.

Surface roughness also influences the solutions: assuming a low surface roughness leads to smaller thermal inertias (TI), and higher levels of surface roughness produce higher TI; If there are sufficient high-quality thermal measurements at shorter wavelengths (short of the thermal emission peak) then the surface roughness can be constrained, otherwise not.

Radiometric sizes using a simple spherical shape (in combination with the object’s spin state) are often of similar quality, only for very strangely-shaped objects or poor coverage in thermal data the radiometric sizes via spherical shapes are off by a few percent (as a general rule, the uncertainty is on the level of 10%).

If all thermal data are taken from before (or only after) opposition then the thermal properties (thermal inertia and roughness) are only poorly constrained (even for cases where

a highly reliable shape/spin solution is available) and the corresponding radiometric sizes are more uncertain (again: maybe closer to 10% accuracy).

In this section, we have performed a similar scaling experiment for different shape models, just like the previous one with occultations, but now using thermal models. In order to evaluate the goodness of the shape model fit to the data, we compare the resulting χ^2 of the different solutions. As explained above, and unlike the results obtained with occultations, there is not a general rule correlating the shape model used with the quality of the fit. In other words, although generally convex and nonconvex shape solutions provide better fits to the data, there are also other cases where sphere shape model fit equally well. Next, we briefly describe the results obtained for each asteroid tested. Volumes are calculated using D_{eff} and the volume uncertainty is calculated assuming a 10% accuracy in the radiometric sizes (the true radiometric size error could be smaller and in many cases closer to 5%, but that requires a more detailed study). Table 5 summarizes the results of the parameters used to fit the data.

- 6 Hebe
Best solution to explain the thermal data: convex solution (from DAMIT) with $TI = 70$, $D_{eff} = 198.1$ km, $pV = 0.24$, indicating an intermediate roughness. The resulting volume estimate is $V = (4.07 \pm 1.22) \cdot 10^{15} m^3$.
- 9 Metis
Preferred solution (acceptable χ^2): convex solution (from DAMIT) with $TI = 15$, $D_{eff} = 177$ km, $pV = 0.18$, low roughness, but the thermal dataset is not great (no IRAS, no Herschel, no WISE). The resulting volume estimate is $V = (2.90 \pm 0.87) \cdot 10^{15} m^3$, in agreement within uncertainty with the volume obtained from occultation.
- 159 Aemilia
Preferred solution: convex and SAGE (both spin-solutions are similar) with $TI = 50$; $D_{eff} = 137.4$ km, $pV = 0.054$, which indicate an intermediate roughness. The resulting volume estimate is $V = (1.36 \pm 0.52) \cdot 10^{15} m^3$, in agreement within uncertainty with the volume obtained from occultation.
- 227 Philosophia
All three shape solutions seem to work (similar χ^2 minimum), but the SAGE has the best-constrained solution (narrow χ^2 minimum), with $TI = 50$, $D_{eff} = 96.7$, $pV = 0.044$, default roughness. The resulting volume estimate is $V = (4.73 \pm 1.42) \cdot 10^{14} m^3$.
- 324 Svea
Preferred solution (best χ^2): convex solution (from DAMIT) with $TI = 75$, $D_{eff} = 77.5$ km, $pV = 0.055$, default roughness. The resulting volume estimate is $V = (2.44 \pm 0.73) \cdot 10^{14} m^3$, in agreement within uncertainty with the volume obtained from occultation.
- 478 Tergeste
The SAGE model is clearly favoured and significantly better than convex or sphere solutions. Best solution at $TI = 75$, $D_{eff} = 87.3$ km, $pV = 0.154$, with intermediate roughness. The resulting volume estimate is $V = (3.48 \pm 1.04) \cdot 10^{14} m^3$.

- 487 Venetia

The SAGE model best fits, with $TI = 100$, $D_{eff} = 69$ km, $pV = 0.21$, intermediate roughness. Interestingly, both convex solutions are worse than a spherical shape. The resulting volume estimate is $V = (1.72 \pm 0.52) \cdot 10^{14} m^3$.

Shape model	χ^2 min	χ^2 lim	Thermal inertia range [$Jm^{-2}s^{-0.5}K^{-1}$]	Diameter range [km]	pV range	Solution evaluation
6 Hebe						
Sphere	1.04	1.30	18 - 93	197.7 - 203.4	0.240 - 0.226	Acceptable
Convex	0.62	0.83	22 - 138	195.0 - 200.8	0.247 - 0.233	Best
ADAM	0.77	0.86	13 - 66	193.9 - 198.4	0.250 - 0.235	Acceptable
9 Metis						
Sphere	4.98	5.73	96 - 230	187.0 - 204.0	0.160 - 0.130	Bad chi2
Convex	1.51	2.30	1 - 41	161.0 - 187.0	0.210 - 0.160	Acceptable
ADAM	1.76	2.51	18 - 61	166.0 - 186.0	0.200 - 0.160	Bad chi2
SAGE	3.14	3.89	47 - 105	170.0 - 179.0	0.190 - 0.160	Bad chi2
159 Aemilia						
Sphere	1.15	1.40	1 - 170	131.6 - 150.2	0.058 - 0.044	Acceptable
Convex	0.44	0.75	1 - 134	130.1 - 147.6	0.060 - 0.047	Best
SAGE	0.44	0.72	1 - 147	129.5 - 148.1	0.061 - 0.046	Best
227 Philosophia						
Sphere	1.24	1.49	84 - 238	106.6 - 109.9	0.036 - 0.034	Acceptable
Convex	1.22	1.47	97 - 272	103.2 - 106.6	0.038 - 0.036	Acceptable
SAGE	1.28	1.53	28 - 95	96.1 - 97.8	0.044 - 0.043	Acceptable
329 Svea						
Sphere	1.50	1.64	88 - 215	74.2 - 79.5	0.060 - 0.052	Bad chi2
Convex	0.94	1.12	6 - 144	74.6 - 79.7	0.059 - 0.052	Best
SAGE	1.09	1.23	74 - 208	72.2 - 77.5	0.063 - 0.055	Acceptable
478 Tergeste						
Sphere	1.67	1.84	65 - 168	88.4 - 97.1	0.146 - 0.121	Bad chi2
Convex	1.52	1.99	26 - 82	81.8 - 90.6	0.174 - 0.142	Bad chi2
SAGE	0.94	1.21	46 - 102	85.1 - 92.8	0.162 - 0.136	Best
487 Venetia						
Sphere	1.09	1.24	186 - 570	71.2 - 75.6	0.197 - 0.175	Acceptable
Convex	1.82	1.93	5 - 38	61.3 - 63.2	0.264 - 0.248	Bad chi2
SAGE	1.04	1.18	67 - 236	67.3 - 70.9	0.220 - 0.199	Best

- χ^2 min: is the minimum of the reduced χ^2 from the match between the model predictions (based on a specific model solution) and all observed fluxes. Reduced χ^2 minima should be reasonably close to 1.0 to accept a fit.
- χ^2 lim: is the $3\text{-}\sigma$ limit. This works only if the reduced χ^2 minimum is reasonably close to 1.0.
- Thermal inertia range: the full possible range for the thermal inertia, where the lower values are connected to a low surface roughness, while the higher ones are connected to a higher surface roughness.
- Diameter range: full $3\text{-}\sigma$ range of possible effective sizes (of an equal-volume sphere).
- pV range: full $3\text{-}\sigma$ range of possible albedos.

Table 5: Results of the thermal modeling for different asteroid shape models.

6 Discussion and conclusion

This document has helped us to review the state of the art in GPs modeling and volume determination. We have gathered together the available photometry, stellar occultation timings and thermal data of a selected subset of the GPs list. Importantly, we have shown that the shape model chosen for size determination has an important impact on the results. In particular, for stellar occultations, we have shown that the uncertainty in size can be even three times greater when using a simple spherical model. For the radiometric technique the assumption of a spherical shape still provides good-quality sizes, but the radiometric size accuracy depends on the quantity and quality of the available thermal measurements. Obtaining the most precise diameter estimates is crucial for volume determinations because the relative error in diameter propagates three-fold into the volume ($V \propto D^3$), and is added quadratically to the mass uncertainty when computing density error bars.

For the selected asteroids which have both occultation chords and thermal data, we have found that sizes and volumes derived from these two independent techniques are in good agreement within uncertainty. As we aim to provide high quality densities of GPs – taking profit of the accurate masses to be provided by Gaia – we have confirmed that it is a necessary effort to derive complex shape models (and reliable spin-state solutions) of the selected targets in order to fulfill our quality expectations. We also demonstrated that the different scaling methods for the volume determination are complementary and help to derive realistic error bars for the volumes and hence for the densities.

7 References

- Bartczak, P., Michałowski, T., Santana-Ros, T., Dudziński, G., 2014, *Monthly Notices of the Royal Astronomical Society*, 443, 1802
- Bartczak, P., Dudziński, G., 2017, *Monthly Notices of the Royal Astronomical Society*, In press
- Braga-Ribas, F., et al. 2014, *Nature*, 508, 72
- Connely, R., & Ostro, S. J., 1984, *Geometriae Dedicata*, 17, 87
- Colas, F., et al. 2012, *Proceedings of the Asteroids, Comets, Meteors 2012 conference*, 6427
- Delbo, M., et al. 2015, *Asteroids IV*, Patrick Michel, Francesca E. DeMeo, and William F. Bottke (eds.), University of Arizona Press, Tucson, p.107-128
- Dunham, D.W. et al. 2017, *Asteroid Occultations V1.0*, NASA Planetary Data System 2017
- Āurech, J., et al. 2007, *Astronomy and Astrophysics*, 465, 331
- Kaasalainen, M., Torppa, J. 2001, *Icarus*, 153, 24
- Kaasalainen, M., Torppa, J. Muinonen, K., 2001, *Icarus* 153, 37
- Marciniak, A., et al. 2011, *Astronomy and Astrophysics*, 529, A107
- Marciniak, A., et al. 2012, *Astronomy and Astrophysics*, 545, A131
- Marciniak, A., et al. 2017, *Astronomy and Astrophysics*, In press
- Marsset, M., et al. 2017, *Astronomy and Astrophysics*, 604, 12
- Michałowski, T., 1993, *Icarus*, 106, 563
- Mouret, S., Hestroffer & D., Mignard, F., 2008, *Planetary and Space Science*, 56, 1819
- Müller, T. et al. 2017, *Astronomy and Astrophysics*, 599, A103
- Ortiz, J.L., et al. 2017, *Nature*, 550, 219
- Santana-Ros, T., Dudziński G., Bartczak, P., 2017, *Astrophysics and Space Science Proceedings*, 46, 55
- Santos-Sanz, P., et al. 2016, *PASP*, 128, 018011
- Torppa, J., et al. 2008, *Icarus*, 198, 91
- Viikinkoski, M., Kaasalainen, M., Āurech, J., 2015a, *Astronomy and Astrophysics*, 576, A8

A Appendix I

Asteroid	Observation date	Major axis (km)	Minor axis (km)	Angle between ellipsoid axes (degrees)	Number of positive chords
13 Egeria	1992-01-08	217	196	0	n.d.
13 Egeria	2008-01-22	215	192	90	8
13 Egeria	2009-01-29	208	208	0	1
13 Egeria	2010-05-13	244	175	64	2
13 Egeria	2010-11-15	215	215	0	1
13 Egeria	2011-09-05	215	215	0	1
13 Egeria	2011-11-17	215	215	0	1
13 Egeria	2012-10-30	215	215	0	1
13 Egeria	2013-03-26	215	215	0	3
13 Egeria	2015-09-19	215	215	0	1
14 Irene	1982-12-13	191	191	0	1
14 Irene	1988-02-24	182	182	0	2
14 Irene	1996-01-24	188	135	2	2
14 Irene	2001-11-21	182	182	0	1
14 Irene	2004-04-16	182	182	0	n.d.
14 Irene	2013-08-02	164	118	-22	3
20 Massalia	2003-12-02	150	150	0	1
20 Massalia	2009-04-22	157	157	0	2
20 Massalia	2012-04-09	131	131	0	1
20 Massalia	2012-10-09	77	94	94	5
60 Echo	2004-08-28	60	60	0	1
60 Echo	2011-05-12	60	60	0	1
60 Echo	2015-09-12	59	59	0	1
64 Angelina	2004-07-03	53	48	-55	6
68 Leto	1999-05-23	151	126	-34	3
68 Leto	2003-05-05	174	178	-34	2
113 Amalthea	n.d.	n.d.	n.d.	n.d.	n.d.

Asteroid	Observation date	Major axis (km)	Minor axis (km)	Angle between ellipsoid axes (degrees)	Number of positive chords
114 Kassandra	2003-12-21	99	99	0	2
114 Kassandra	2005-05-21	100	100	0	n.d.
114 Kassandra	2010-02-21	99	99	0	1
114 Kassandra	2011-07-07	99	99	0	1
114 Kassandra	2014-03-11	97	70	-77	2
145 Adeona	2002-07-09	151	151	0	1
145 Adeona	2005-02-02	193	103	90	6
145 Adeona	2010-04-21	151	151	0	1
145 Adeona	2011-07-19	151	151	0	1
145 Adeona	2015-11-16	141	141	0	1
162 Laurentia	1999-09-21	99	99	0	n.d.
162 Laurentia	2005-12-01	97	97	0	4
162 Laurentia	2008-04-23	103	103	0	n.d.
162 Laurentia	2013-02-28	85	85	0	1
297 Caecilia	2007-04-16	39	39	0	2
308 Polyxo	2000-01-10	165	126	39	5
308 Polyxo	2004-01-29	140	140	0	2
308 Polyxo	2010-06-02	141	141	0	3
308 Polyxo	2015-06-27	135	135	0	1
381 Myrrha	1991-01-13	148	116	-85	25
381 Myrrha	2014-03-12	148	148	0	1
381 Myrrha	2015-04-14	148	116	0	1
402 Chloe	2003-09-01	54	54	0	1
402 Chloe	2004-12-15	76	55	-64	3
402 Chloe	2004-12-23	75	61	-85	2
402 Chloe	2006-05-21	54	54	0	n.d.
402 Chloe	2008-12-08	54	54	0	1
402 Chloe	2010-05-11	54	54	0	1
402 Chloe	2015-06-07	60	60	0	1

Asteroid	Observation date	Major axis (km)	Minor axis (km)	Angle between ellipsoid axes (degrees)	Number of positive chords
441 Bathilde	2003-01-11	67	47	-83	5
441 Bathilde	2004-04-01	70	70	0	1
441 Bathilde	2009-10-13	70	70	0	1
441 Bathilde	2014-07-19	59	59	0	1
441 Bathilde	2014-09-30	78	59	70	1
441 Bathilde	2014-10-13	73	59	80	1
636 Erika	2009-10-13	74	74	0	1
636 Erika	2014-12-01	73	73	0	n.d.
636 Erika	2015-01-08	74	74	0	1
654 Zelinda	1995-01-19	133	120	0	n.d.
654 Zelinda	1995-02-13	127	127	0	n.d.
654 Zelinda	2001-09-28	133	133	0	1
654 Zelinda	2002-03-27	138	103	-40	3
654 Zelinda	2003-07-29	120	120	0	2
654 Zelinda	2007-07-13	129	129	0	1
654 Zelinda	2007-09-10	129	129	0	3
654 Zelinda	2007-11-16	122	122	0	n.d.
654 Zelinda	2009-02-07	129	129	0	n.d.
654 Zelinda	2009-03-16	129	120	0	3
654 Zelinda	2010-05-04	129	129	0	1
654 Zelinda	2010-08-02	129	129	0	2
654 Zelinda	2011-05-15	129	129	0	1
654 Zelinda	2012-01-06	145	110	28	7
654 Zelinda	2013-05-12	124	108	-39	4
654 Zelinda	2015-12-31	137	119	-66	5

Asteroid	Observation date	Major axis (km)	Minor axis (km)	Angle between ellipsoid axes (degrees)	Number of positive chords
704 Interamnia	1984-08-05	331	300	0	1
704 Interamnia	1990-12-09	331	300	0	n.d.
704 Interamnia	1995-12-06	316	316	0	1
704 Interamnia	1996-12-17	343	323	83	9
704 Interamnia	2003-03-23	350	303	84	46
704 Interamnia	2006-06-01	317	317	0	1
704 Interamnia	2007-09-09	357	311	67	6
704 Interamnia	2009-01-11	334	315	98	3
704 Interamnia	2011-04-11	357	357	0	1
704 Interamnia	2011-07-02	357	357	0	1
704 Interamnia	2011-11-05	300	300	0	2
704 Interamnia	2012-11-12	331	262	63	4
704 Interamnia	2012-12-02	339	339	0	2
721 Tabora	n.d.	n.d.	n.d.	n.d.	n.d.
1427 Ruvuma	2010-10-16	40	40	0	1

Table 6: Existing occultation observations of the selected targets with a crude estimation of their sizes by using an ellipsoid to fit the data.